J Solid State Electrochem (2013) 17:1393–1399
DOI 10.1007/s10008-013-2005-7

ORIGINAL PAPER

Improvement of cyclability of silicon-containing carbon nanofiber anodes for lithium-ion batteries by employing succinic anhydride as an electrolyte additive

Ying Li · Guanjie Xu · Yingfang Yao · Leigang Xue · Shu Zhang · Yao Lu · Ozan Toprakci · Xiangwu Zhang

Received: 3 October 2012 / Revised: 8 January 2013 / Accepted: 14 January 2013 / Published online: 27 January 2013

Abstract Si/C composite nanofibers were prepared by electrospinning and carbonization using polyacrylonitrile as the spinning medium and carbon precursor. The effect of electrolyte additive succinic anhydride (SA) on the electrochemical performance of Si/C composite nanofiber anodes was investigated. Results show that after 50 cycles, the discharge capacity of Si/C composite nanofiber anode with the SA-added electrolyte is 34 % higher than that with additive-free electrolyte. At 150th cycle, the capacity retention of Si/C composite nanofiber anode with SA-added electrolyte is 82 % under 70 % state-of-charge. It is demonstrated that adding additive SA in the electrolyte is an effective and economic way to improve the cyclability of high-capacity Si/C composite nanofibers for next-generation high-energy lithium-ion batteries.

Keywords Electrospinning · Carbon nanofiber · Si nanoparticle · Succinic anhydride · Lithium-ion batteries

Introduction

Commercial lithium-ion batteries use graphite (theoretical capacity, 372 $mAhg^{-1}$) as the anode material [1]. To develop rechargeable lithium-ion batteries with high energy densities, Si has been studied extensively due to its extremely large capacity of 3,579 $mAhg^{-1}$, corresponding to the formation of $Li_{15}Si_4$ [2–4]. However, the relatively low electric conductivity and large volume change of Si particles limit the use of Si anodes in practical batteries. A rapid capacity fading is often observed for Si anodes during charge/discharge cycling due to the mechanical failure and loss of effective electronic contacts, which were caused by the large volume changes of active Si particles.

Several approaches have been developed to improve the cyclability of Si anodes, such as using nanosized Si particles and nanowires, dispersing Si into inactive/active matrix, controlling the cycling conditions of the battery, etc. [4–9]. Recently, a new Si/C composite nanofiber anode was developed by embedding Si nanoparticles in electrospun carbon nanofibers [10–13]. The carbon nanofiber matrix can accommodate the volume change of Si during cycling, and hence, Si/C composite nanofiber anode has the potential to combine the advantages of carbon (long cycle life) and silicon (high storage capacity) materials. Results show that the initial capacity of Si/C composite nanofibers is around 1,000 $mAhg^{-1}$; however, the capacity retention is not satisfactory yet and more work is needed to improve the cyclability of the Si/C composite nanofiber anode[14–16].

To improve the cyclability of Si/C composite nanofibers, it is important to control the interfacial properties. The use of electrolyte additive is a relatively economic and effective way to achieve high performance for Si/C composite nanofiber anodes by improving the interfacial stability. The electrolyte additive can facilitate the formation of a stable solid electrolyte interface (SEI) film on the surface of the electrode material, which could help prevent the further reaction between the electrolyte and active material during cycling. Various spectroscopic measurements have identified that the SEI film is mainly formed by the decomposed products of electrolyte solvents and salts, such as hydrocarbons, lithium alkyl carbonates, LiOH, Li_2CO_3, and other salt moieties like

Y. Li · G. Xu · Y. Yao · L. Xue · S. Zhang · Y. Lu · O. Toprakci · X. Zhang (✉)
Fiber and Polymer Science Program, Department of Textile Engineering, Chemistry and Science, North Carolina State University, Raleigh, NC 27695-8301, USA
e-mail: xiangwu_zhang@ncsu.edu

LiF for $LiPF_6$-based electrolytes [17, 18]. Up till now, only a few additives have been studied, such as fluoroethylene carbonate (FEC), vinylene carbonate (VC), polyether modified siloxanes, succinic anhydride (SA), etc. [19–23]. Recently, McArthur and his co-workers investigated the SEI growth by using an in situ spectroscopic ellipsometry method [24]. It was found that the SEI film became thicker by the introduction of FEC or VC additive. The electrode–electrolyte interphases play an important role in determining the performance of LIBs. The electrode–electrolyte interphases formed by carbon-based anode materials are solvent sensitive due to the weak Van der Waals interactions of the layer structure [25]. For Si-based materials, the mechanism of interphase formation is different from that of carbon materials. Hence, it is important to investigate the behavior of SEI in Si/C composite systems. However, most current SEI work focuses on the Si thin film, which behaves differently from anodes that contain Si nanoparticles.

In this work, we investigated the effect of SA as an electrolyte additive on the electrochemical performance of Si/C composite nanofiber anodes. The chemical structure of SA is shown in Fig. 1. The use of additive SA helped preserve the integrity of the electrode structure, and as a result, the capacities and cycling performance of Si/C composite nanofiber anodes for high-energy lithium-ion batteries have been improved significantly.

Experimental

Electrode preparation

Electrospun Si/C composite nanofibers were prepared as an anode material for lithium-ion batteries. Polyacrylonitrile (PAN, Pfaltz & Bauer Inc., 150,000 $g mol^{-1}$) was used as the spinning media and carbon source. Si nanoparticles with a diameter of 30–50 nm were received from Nanostructured & Amorphous Materials, Inc without further purification.

Si nanoparticles (15 wt%) were added into a PAN solution (8 wt%) in *N*,*N*-dimethylformamide (Aldrich) and were stirred at 60 °C for 24 h, followed by ultrasonic treatment for 1 h to obtain a homogenous dispersion. A variable high-voltage power supply (Gamma ES40P-20 W/DAM) was used to provide a high voltage (18 kV) for electrospinning. The flow rate used was 0.75 $mL h^{-1}$, and the needle-to-collector distance was 15 cm. Electrospun fibers were collected on an aluminum foil.

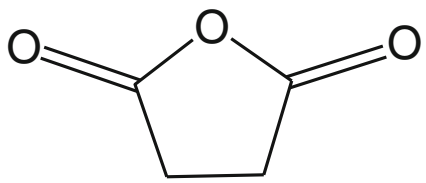

Fig. 1 Chemical structure of succinic anhydride

Electrospun Si/PAN precursor nanofibers were stabilized in air environment at 280 °C for 5 h (heating rate, 5 °C/min), and then they were carbonized at 800 °C for 2 h in argon atmosphere (heating rate, 2 °C/min) to form Si/C composite nanofibers.

Nanofiber characterization

The morphology of composite nanofibers was examined by field emission scanning electron microscope (FESEM-JEOL 6400F SEM at 5 kV). The structure of composite nanofibers was also investigated by wide-angle X-ray diffraction (Philips X'Pert PRO MRD HR X-Ray Diffraction System). Composition analysis of the SEI layer on composite nanofiber surface was performed using X-ray photoelectron spectroscopy (XPS) after the first cycle.

Electrochemical measurements

Two electrolytes were prepared: (1) 1 M $LiPF_6$ in ethylene carbonate (EC)/diethyl carbonate (DEC)/dimethyl carbonate (DMC; 1/1/1, *v*/*v*/*v*) without SA, and (2) 1 M $LiPF_6$ in EC/DEC/DMC (1/1/1, *v*/*v*/*v*) with 3 wt% additive SA. These two electrolytes are denoted as 1 M $LiPF_6$/EC+DEC+DMC and 1 M $LiPF_6$/SA/EC+DEC+DMC, respectively.

Anodes were prepared by two methods. In the first method, the Si/C nanofiber mat was directly used as the anode without adding polymer binder or carbon black. In the second method, the anode was prepared by mixing 80 % ground Si/C nanofibers with 10 % polyamide imide (PAI) binder and 10 % carbon black. Si/C composite nanofiber anodes were then assembled into CR2032-type coin cells with the above-mentioned electrolytes. The mass loadings of the active material were in the range of 2–3 mg/cm^2. Lithium metal was used as the counter electrode and Celgard 2400 membrane as the separator.

Cyclic voltammetry (CV) measurements were performed on a Gamry Reference 600 Potentiostat/Galvanostat/ZRA with the voltage ranging from 0.05 to 3.0 V at a scan rate of 0.05 mV/s. Electrochemical impedance spectra (EIS) were obtained using the Gamry Reference 600 Potentiostat/Galvanostat/ZRA in a 10.0-mV AC voltage signal in the 10^6–10^{-2} Hz frequency range. Before each EIS measurement, the electrodes were first charged galvanostatically at 50 $mA g^{-1}$ to 0.05 V, and then remained at open circuit for 5.0 h to allow their potential to stabilize. Galvanostatic charge–discharge experiments were carried out using an Arbin automatic battery cycler at a current density of 50 or 100 $mA g^{-1}$ between 0.01 and 1.5 V.

Results and discussion

Morphology and structure of Si/C composite nanofibers

Figure 2 shows typical SEM images of 15 wt% Si/PAN precursor nanofibers. All nanofibers are continuous and uniform with Si nanoparticles distributed along the fiber direction. It is also seen that some Si nanoparticles form clusters on the fiber surface.

After carbonization, the PAN matrix was converted to carbon and Si/C nanofibers were formed. Figure 3 shows SEM images of the resultant Si/C nanofibers, which were carbonized at 800 °C. Compared with the corresponding Si/PAN precursor shown in Fig. 2, Si/C nanofibers have more Si nanoparticles exposed on the surface. The diameters of all composite nanofibers are in the range of 150 to 250 nm.

WAXRD measurement was conducted to evaluate the structure evolution of Si/C composite nanofibers (Fig. 4). It is seen that Si nanoparticles show clear diffractions at 28.4°, 47.4°, 56.2°, 69.2°, 76.5°, and 88.1° [5, 26]. After incorporating Si nanoparticles into the carbon matrix, the resultant Si/C nanofibers still exhibit the same peaks, but

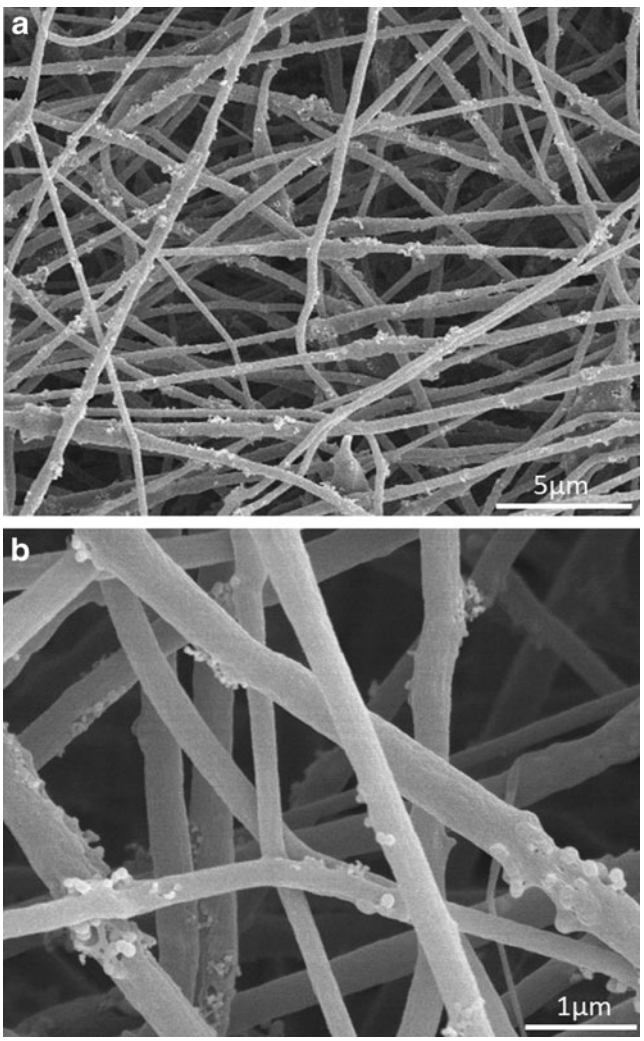

Fig. 2 SEM images of 15 wt% Si/PAN precursor nanofibers

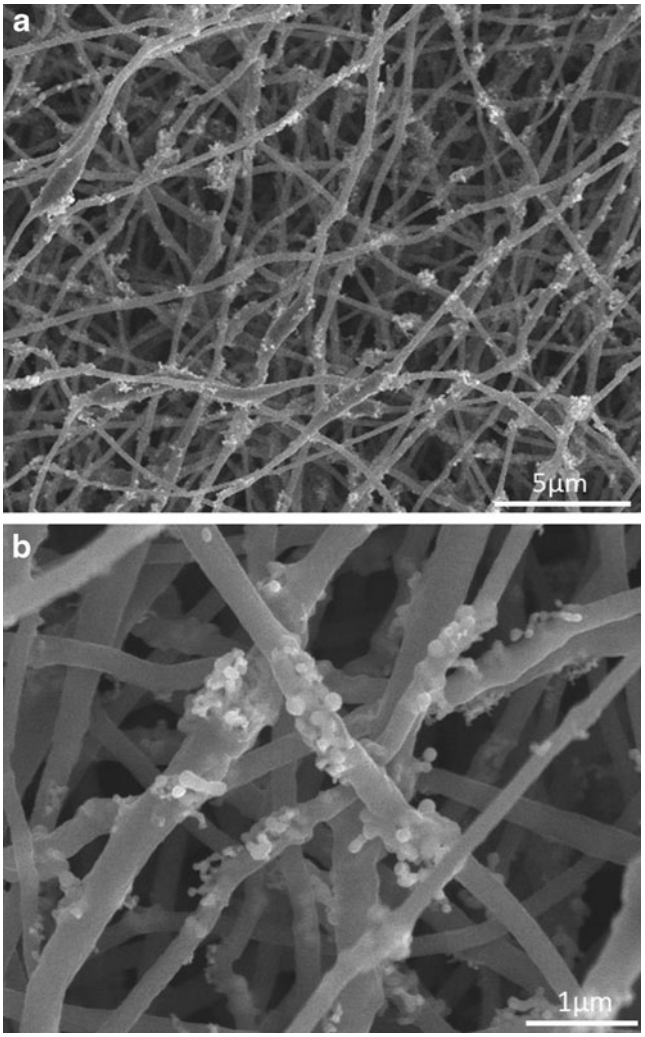

Fig. 3 SEM images of Si/C composite nanofibers prepared from 15 wt% Si/PAN precursor

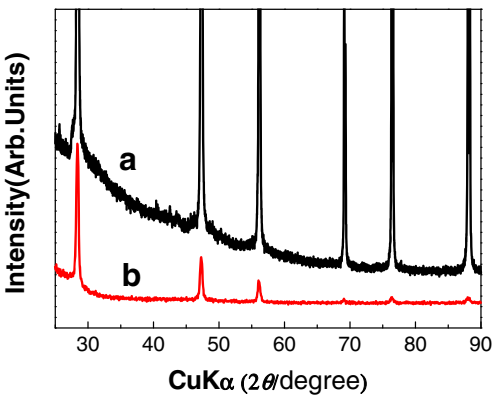

Fig. 4 XRD patterns of (*a*) Si nanoparticles and (*b*) Si/C composite nanofibers prepared from 15 wt% Si/PAN precursor

with lower intensities. No peaks can be found for SiO_2 or Si-C alloy, indicating that Si was not oxidized and did not react with carbon during the carbonization process.

Electrochemical performance of Si/C nanofiber mat anode

The formation of SEI is a result of the reduction of both solvents and salts. Figure 5 shows the CV curves of the Si/C nanofiber mat anode (without binder and carbon black) in two electrolytes: 1 M $LiPF_6$/EC+DEC+DMC and 1 M $LiPF_6$/SA/EC+DEC+DMC. The potential window used was 0.05–3 V, and the scan rate was 0.05 mV/S. In both electrolytes, a broad cathodic peak appears at the first cycle. This cathodic peak is resulted from the decomposition of the electrolyte and the formation of SEI film, which cause the initial irreversible capacity [28–30]. After the introduction of additive SA in the liquid electrolyte, the cathodic peak shifts from 0.52 to 0.40 V and the peak intensity decreases slightly, which indicate that the SEI film property has been changed by introducing additive SA [27, 30, 31].

Figure 6 shows the XPS spectra for Si/C composite nanofiber anodes after the first cycle. The F 1 s spectra

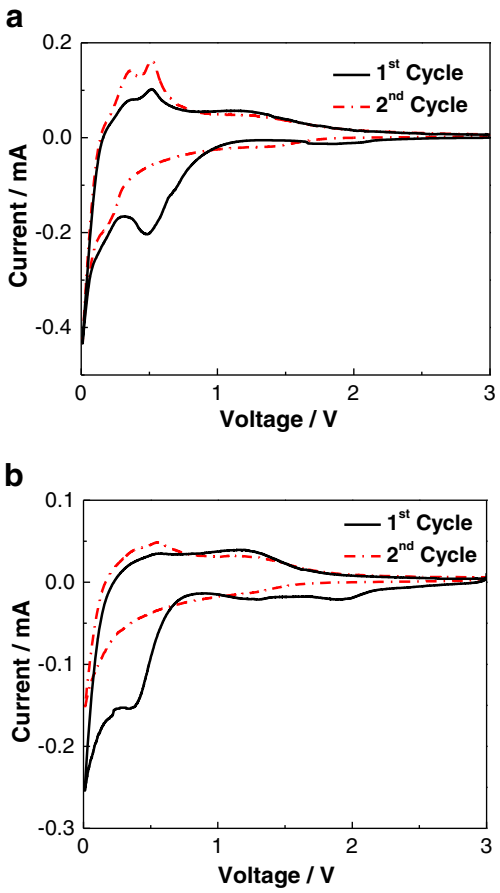

Fig. 5 Cyclic voltammetry profiles of Si/C nanofiber mat anode with two different electrolytes: **a** 1 M $LiPF_6$/EC+DEC+DMC and **b** 1 M $LiPF_6$/SA/EC+DEC+DMC. Scan rate, 0.05 mV/S

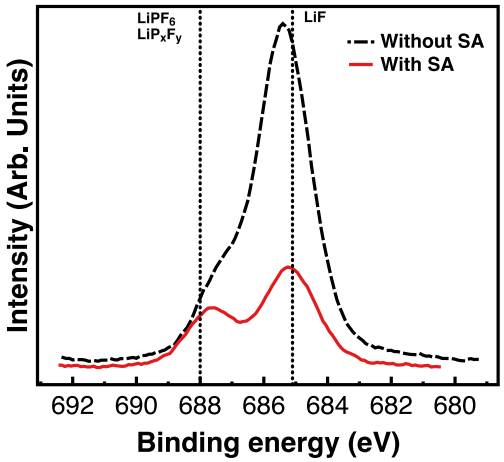

Fig. 6 XPS spectra of Si/C composite nanofiber anodes: F 1 s after the first cycle

show a strong peak at around 685 eV, corresponding to LiF, and a small peak at around 688 eV, corresponding to $LiPF_6$ and LiP_xF_y [32, 33]. It can be seen that the intensities of both peaks are reduced after the introduction of additive SA, which implies that the decomposition of $LiPF_6$ on the surface of composite nanofiber anodes is reduced. SA changes the SEI film property by promoting the formation of Li_2CO_3 and hydrocarbons and prohibiting the decomposition of $LiPF_6$ during cycling [32–34]. From Fig. 5, it is also seen that in both electrolytes, no new SEI formation can be observed at the second cycle.

Figure 7 displays the impedance spectra of the Si/C nanofiber mat anode in two electrolytes. In both electrolytes, the nanofiber anode shows one high and intermediate frequency semicircle and a straight line in the low-frequency range, corresponding to the migration within the surface layer, the interfacial charge-transfer impedance, and lithium diffusion in the electrode, respectively [35, 36]. Zhang et al. has studied the SEI formation process on the graphite electrode and found that the compactness and stability of the SEI film could be evaluated by measuring the ionic conductivity of SEI [27, 37]. The ionic conduction of the SEI film is a result of the migration of solvated Li ions through the micro-pores of SEI since the dried SEI itself is neither electronic conductive nor ionic conductive [27, 28, 37]. Hence, higher resistance corresponds to a more compact and more stable SEI. As shown in Fig. 7, with the introduction of additive SA, the diameter of the depressed semicircle is increased, which indicates the increase in charge transfer resistance. The interfacial resistance of the Si/C composite nanofiber anode in 1 M $LiPF_6$/SA/EC+DEC+DMC is larger than that in 1 M $LiPF_6$/EC+DEC+DMC, which means the SEI structure has become more compact and less conductive by the introduction of additive SA in the electrolyte. In Fig. 7, the intersection in the real axis in high frequency region represents the electrolyte resistance, more strictly

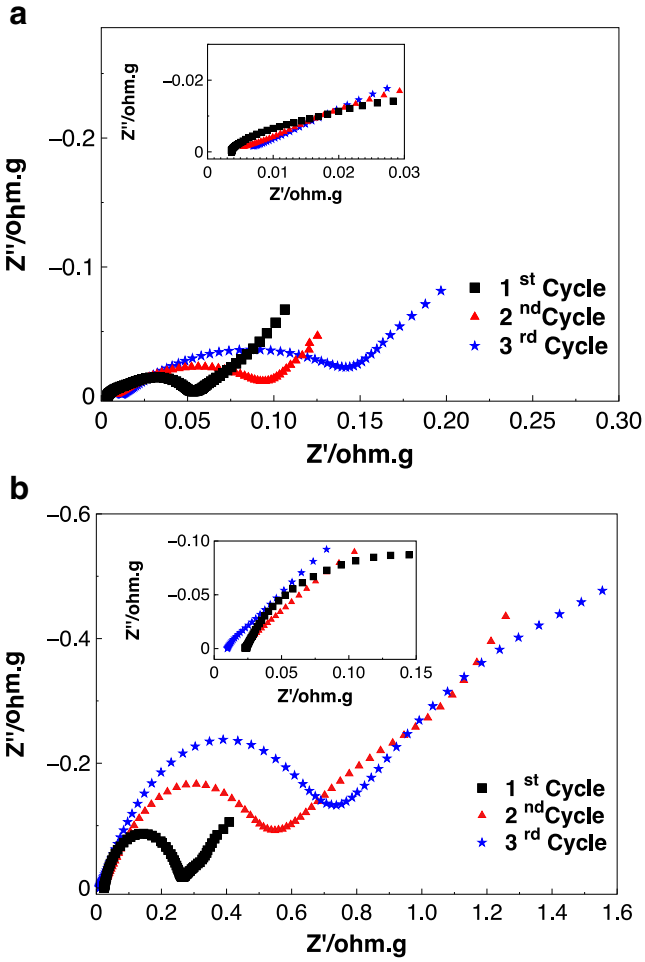

Fig. 7 Nyquist plots of Si/C nanofiber mat anode with two different electrolytes: **a** 1 M $LiPF_6$/EC+DEC+DMC and **b** 1 M $LiPF_6$/SA/EC+DEC+DMC. *Insets* are the enlarged Nyquist plots at high frequencies

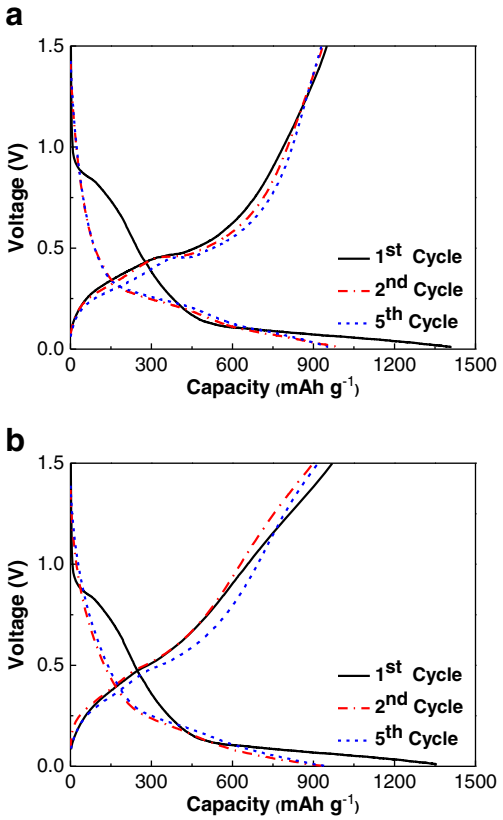

Fig. 8 Galvanostatic charge-discharge curves of Si/C nanofiber mat anode with two different electrolytes: **a** 1 M $LiPF_6$/EC+DEC+DMC, and **b** 1 M $LiPF_6$/SA/EC+DEC+DMC. Current density: 50 mA g^{-1}

including all ohmic resistances. The introduction of SA moves the intersection to the right, indicating that the electrolyte resistance has been increased by SA.

Galvanostatic charge–discharge curves of the Si/C nanofiber mat anode were obtained in two electrolytes, and the results are shown in Fig. 8. The tests were conducted at 50 mA g^{-1} under the 100 % state-of-charge condition by using cutoff voltages of 0.01 and 1.5 V. At the first cycle, the Si/C nanofiber mat anode shows a charge capacity of approximately 1,410 mAh g^{-1} and discharge capacity of 950 mAh g^{-1}, respectively, in 1 M $LiPF_6$/EC+DEC+DMC (Fig. 8a). The corresponding Coulombic efficiency is 67.3 %. In 1 M $LiPF_6$/SA/EC+DEC+DMC, the first-cycle charge and discharge capacities of the Si/C nanofiber mat anode change to 1,370 and 970 mAh g^{-1}, respectively, corresponding to a higher Coulombic efficiency of 71.5 % (Fig. 8b). The formation of SEI occurs in the range of 0.3–0.9 V vs Li^+/Li, and this SEI voltage is sensitive to the current density applied. The galvanostatic charge–discharge curves were measured at a current density of 50 mA g^{-1}, while the cyclic voltammetry data were obtained at a scan rate of 0.05 mV/S. Since the data were obtained at different conditions, the SEI formation voltages are slightly different.

Figure 9a compares the cycling performance of the Si/C nanofiber mat anode in two different electrolytes. It is seen that in the first 10 cycles, the Si/C nanofiber mat anode has comparable capacities in both electrolytes. However, after 10 cycles, the Si/C nanofiber mat anode has higher capacities in 1 M $LiPF_6$/SA/EC+DEC+DMC. For example, at the 50th cycle, the discharge capacity of the Si/C nanofiber mat anode is 598 mAh g^{-1} in 1 M $LiPF_6$/EC+DEC+DMC, and the capacity increases to 802 mAh g^{-1} in 1 M $LiPF_6$/SA/EC+DEC+DMC. The corresponding capacity retentions are 63.0 and 82.8 %, respectively, in these two electrolytes. Results indicate that, at the 50th cycle, the discharge capacity of Si/C composite nanofiber mat anode in 1 M $LiPF_6$/SA/EC+DEC+DMC is 34 % higher than that in 1 M $LiPF_6$/EC+DEC+DMC and more than 2.2 times larger than the theoretical capacity (372 mAh g^{-1}) of graphite, which is the standard anode material for current commercial lithium-ion batteries [1].

The Coulombic efficiencies of the Si/C nanofiber mat anode in two different electrolytes are shown in Fig. 9b. The low Coulombic efficiency in the initial cycle is mainly

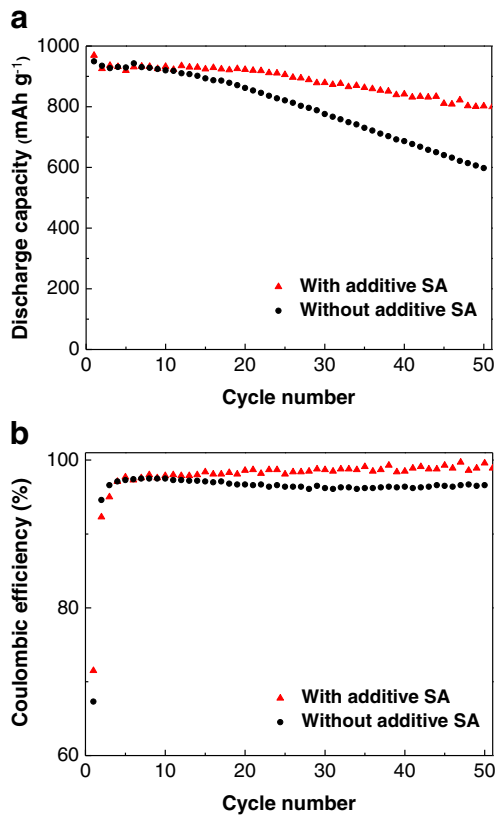

Fig. 9 Cycling performance (**a**) and Coulombic efficiency (**b**) of Si/C nanofiber mat anode with two different electrolytes: 1 M $LiPF_6$/EC+DEC+DMC and 1 M $LiPF_6$/SA/EC+DEC+DMC. Current density, 50 mA g^{-1}

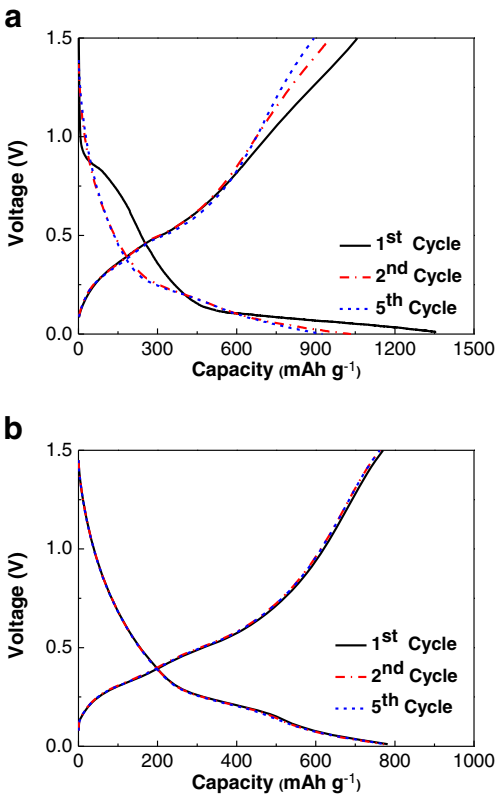

Fig. 10 Galvanostatic charge–discharge curves of PAI-bound Si/C nanofiber anode under two state-of-charge conditions: **a** 100 and **b** 70 %. Current density, 100 mA g^{-1}

caused by the consumption of lithium ions during the SEI formation. It is seen that after 5 cycles, the Coulombic efficiency of the Si/C nanofiber mat anode reaches 97 % in both electrolytes. However, after 10 cycles, the Coulombic efficiency in 1 M $LiPF_6$/EC+DEC+DMC decreases to around 96 %, but that in 1 M $LiPF_6$/SA/EC+DEC+DMC increases to around 98 %. This indicates that the SEI film formed on the Si/C nanofiber mat anode in 1 M $LiPF_6$/EC+DEC+DMC is less stable than that in 1 M $LiPF_6$/SA/EC+DEC+DMC.

From Figs. 8 and 9, it can be concluded that both the Coulombic efficiency and cycling performance of Si/C nanofiber mat anode have been improved by the introduction of SA as an electrolyte additive. The improvement of the electrochemical performance is mainly caused by the formation of a stable SEI film on the surface of Si/C nanofiber mat anode.

Electrochemical performance of PAI-bound Si/C nanofiber anode

In practical lithium-ion batteries, anodes are often prepared by using a polymer binder. Therefore, in order to further investigate the cycling performance in the SA-added electrolyte, Si/C nanofiber anodes were prepared by using PAI as a polymer binder. The electrochemical performance of the PAI-bound Si/C nanofiber anode prepared from 15 wt% Si/PAN precursor was investigated by carrying out galvanostatic charge–discharge cycles under 100 and 70 % state-of-charge conditions at a current density of 100 mA g^{-1}, and the results are shown in Fig. 10. It is seen that at 100 % state-of-charge, the Si/C nanofiber anode shows a specific

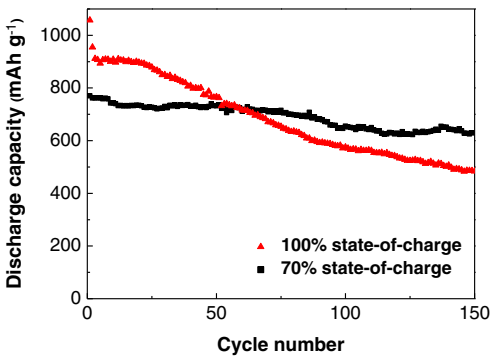

Fig. 11 Comparison of cycling performance of PAI-bound Si/C nanofiber anode under two state-of-charge conditions. Current density, 100 mA g^{-1}

discharge capacity of 1,057 $mAhg^{-1}$ at the first cycle. However, at 70 % state-of-charge cycle, the Si/C nanofiber anode shows a first-cycle discharge capacity of 770 $mAhg^{-1}$, i.e., about 70 % of the capacity at 100 % state-of-charge.

Figure 11 shows the comparison of the cycling performance of the PAI-bound Si/C nanofiber anode under two state-of-charge conditions. The capacity fading at 70 % state-of-charge condition is much slower than that at 100 % state-of-charge. It is seen that during first 57 cycles, the discharge capacity at 100 % state-of-charge is higher than that at 70 % state-of-charge. However, the capacity at 100 % state-of-charge decreases significantly and becomes lower than that at 70 % state-of-charge after 60 cycles. At the 100th and 150th cycles, the discharge capacities at 100 % state-of-charge are only 575.4 and 484 $mAhg^{-1}$, respectively. However, the discharge capacities at 70 % state-of-charge condition are still 650 and 629 $mAhg^{-1}$, respectively, at 100th and 150th cycles, indicating slower capacity fading. The capacity retention of the PAI-bound Si/C nanofiber anode under 70 % state-of-charge is 82 % at the 150th cycle, compared to 46 % for 100 % state-of-charge at the same cycle. The results show that the cyclability of the Si/C nanofiber anode has been improved by using SA-added electrolyte and by carefully controlling the state-of-charge condition.

Conclusions

In this work, the effect of additive SA on the electrochemical performance of Si/C nanofiber anodes made from electrospun Si/PAN precursor was investigated. The use of additive SA could help improve the interfacial properties by preventing the decomposition of $LiPF_6$ salt and preserving the integrity of the electrode structure which are beneficial to improve the electrochemical behavior. The cyclability of Si/C nanofiber anodes could be further improved by careful control of the state-of-charge condition. Results show that the capacity retention of the PAI-bound Si/C nanofiber anode under 70 % state-of-charge is 82 % at the 150th cycle. Therefore, the Coulombic efficiency and cycling performance of Si/C composite nanofiber anodes have both been improved. This indicates that employing additive SA is an effective and economic method to improve the overall electrochemical performance of Si/C composite nanofiber anodes for high-energy lithium-ion batteries.

Acknowledgments This research was supported by the U.S. Department of Energy under Grant No: DE-EE0001177, Advanced Transportation Energy Center, and ERC Program of the National Science Foundation under Award Number EEC-08212121.

References

1. Kaskhedikar NA, Maier J (2009) Adv Mater 21:2664–2680
2. Obrovac MN, Christensen L (2004) Electrochemical and Solid-State Letters 7:A93–A96
3. Obrovac MN, Krause LJ (2007) J Electrochem Soc 154:A103–A108
4. Thakur M, Isaacson M, Sinsabaugh SL, Wong MS, Biswal SL (2012) J Power Sources 205:426–432
5. Wilson AM, Dahn JR (1995) J Electrochem Soc 142:326–332
6. Fleischauer MD, Topple JM, Dahn JR (2005) Electrochemical and Solid-State Letters 8:A137–A140
7. Si Q, Hanai K, Imanishi N, Kubo M, Hirano A, Takeda Y, Yamamoto O (2009) J Power Sources 189:761–765
8. Wei-Jun Z (2011) J Power Sources 196:877–885
9. Zhou X, Yin Y-X, Wan L-J, Guo Y-G (2012) Chem Commun 48:2198–2200
10. Ji L, Jung K-H, Medford AJ, Zhang X (2009) J Mater Chem 19:4992–4997
11. Ji L, Zhang X (2009) Carbon 47:3219–3226
12. Ji L, Zhang X (2009) Electrochem Commun 11:1146–1149
13. Ji L, Zhang X (2010) Energy Environ Sci 3:124–129
14. Gu M, Li Y, Li X, Hu S, Zhang X, Xu W, Thevuthasan S, Baer DR, Zhang J-G, Liu J, Wang C (2012) ACS Nano 6:8439–8447
15. Li Y, Lin Z, Xu G, Yao Y, Zhang S, Toprakci O, Alcoutlabi M, Zhang X (2012) ECS Electrochemistry Letters 1:A31–A33
16. Li Y, Guo B, Ji L, Lin Z, Xu G, Liang Y, Zhang S, Toprakci O, Hu Y, Alcoutlabi M, Zhang X (2013) Carbon 51:185–194
17. Aurbach D, Zaban A, Ein-Eli Y, Weissman I, Chusid O, Markovsky B, Levi M, Levi E, Schechter A, Granot E (1997) J Power Sources 68:91–98
18. Aurbach D, Ein-Eli Y (1995) J Electrochem Soc 142:1746–1752
19. Choi N-S, Yew KH, Lee KY, Sung M, Kim H, Kim S-S (2006) J Power Sources 161:1254–1259
20. Aurbach D, Gnanaraj JS, Geissler W, Schmidt M (2004) J Electrochem Soc 151:A23–A30
21. Inose T, Tada S, Morimoto H, Tobishima S-I (2006) J Power Sources 161:550–559
22. Han GB, Ryou MH, Cho KY, Lee YM, Park JK (2010) J Power Sources 195:3709–3714
23. Ota H, Sakata Y, Otake Y, Shima K, Ue M, Yamaki J-i (2004) J Electrochem Soc 151:A1778–A1788
24. McArthur MA, Trussler S, Dahn JR (2012) J Electrochem Soc 159:A198–A207
25. Xu K, von Cresce A (2011) J Mater Chem 21:9849–9864
26. Hu Y-S, Demir-Cakan R, Titirici M-M, Müller J-O, Schlögl R, Antonietti M, Maier J (2008) Angew Chem Int Ed 47:1645–1649
27. Zhang SS, Ding MS, Xu K, Allen J, Jow TR (2001) Electrochemical and Solid State Letters 4:A206–A208
28. Zhang SS (2006) J Power Sources 162:1379–1394
29. Chan CK, Ruffo R, Hong SS, Huggins RA, Cui Y (2009) J Power Sources 189:34–39
30. Yen Y-C, Chao S-C, Wu H-C, Wu N-L (2009) J Electrochem Soc 156:A95–A102
31. Chan CK, Ruffo R, Hong SS, Cui Y (2009) J Power Sources 189:1132–1140
32. Lee YM, Lee JY, Shim H-T, Lee JK, Park J-K (2007) J Electrochem Soc 154:A515–A519
33. Etacheri V, Haik O, Goffer Y, Roberts GA, Stefan IC, Fasching R, Aurbach D (2011) Langmuir 28:965–976
34. Andersson AM, Abraham DP, Haasch R, MacLaren S, Liu J, Amine K (2002) J Electrochem Soc 149:A1358–A1369
35. Zhang X-W, Patil PK, Wang C, Appleby AJ, Little FE, Cocke DL (2004) J Power Sources 125:206–213
36. Wang L, Yu Y, Chen P-C, Chen C-H (2008) Scr Mater 58:405–408
37. Zhang SS, Xu K, Jow TR (2006) Electrochim Acta 51:1636–1640